February 2006

Two-Step Sintering of Ceramics with Constant Grain-Size, II: $BaTiO_3$and Ni–Cu–Zn Ferrite

X.-H. Wang
Tsinghua University

X.-Y. Deng
Tsinghua University

Hai-Lin Bai
Tsinghua University

H. Zhou
Tsinghua University

Wei-Guo Qu
Tsinghua University

See next page for additional authors

Two-Step Sintering of Ceramics with Constant Grain-Size, II: $BaTiO_3$and Ni–Cu–Zn Ferrite

Abstract
We investigated the preparation of bulk dense nanocrystalline $BaTiO_3$ and Ni–Cu–Zn ferrite ceramics using an unconventional two-step sintering strategy, which offers the advantage of not having grain growth while increasing density from about 75% to above 96%. Using nanosized powders, dense ferrite ceramics with a grain size of 200 nm and $BaTiO_3$ with a grain size of 35 nm were obtained by two-step sintering. Like the previous studies on Y_2O_3, the different kinetics between densification diffusion and grain boundary network mobility leaves a kinetic window that can be utilized in the second-step sintering. Evidence indicates that low symmetry, ferroelectric structures still exist in nanograin $BaTiO_3$ ceramics, and that saturation magnetization is the same in nanograin and coarse grain ferrite ceramics.

Author(s)
X.-H. Wang, X.-Y. Deng, Hai-Lin Bai, H. Zhou, Wei-Guo Qu, L.-T. Li, and I-Wei Chen

journal

J. Am. Ceram. Soc., 89 [2] 438–443 (2006)
DOI: 10.1111/j.1551-2916.2005.00728.x

Two-Step Sintering of Ceramics with Constant Grain-Size, II: $BaTiO_3$ and Ni–Cu–Zn Ferrite

X.-H. Wang, X.-Y. Deng, Hai-Lin Bai, H. Zhou, Wei-Guo Qu, and L.-T. Li

State Key Laboratory of New Ceramics and Fine Processing, Department of Materials Science and Engineering, Tsinghua University, Beijing 100084, China

I.-W. Chen†

Department of Materials Science and Engineering, University of Pennsylvania, Philadelphia, Pennsylvania19104-5272

We investigated the preparation of bulk dense nanocrystalline $BaTiO_3$ and Ni–Cu–Zn ferrite ceramics using an unconventional two-step sintering strategy, which offers the advantage of not having grain growth while increasing density from about 75% to above 96%. Using nanosized powders, dense ferrite ceramics with a grain size of 200 nm and $BaTiO_3$ with a grain size of 35 nm were obtained by two-step sintering. Like the previous studies on Y_2O_3, the different kinetics between densification diffusion and grain boundary network mobility leaves a kinetic window that can be utilized in the second-step sintering. Evidence indicates that low symmetry, ferroelectric structures still exist in nanograin $BaTiO_3$ ceramics, and that saturation magnetization is the same in nanograin and coarse grain ferrite ceramics.

I. Introduction

Two-step sintering is a promising approach to obtain fully dense nanograin ceramics because it suppresses grain growth in the final stage of sintering.[1] This was demonstrated for Y_2O_3, which has a cubic, defective fluorite structure, and for Y_2O_3 doped with either Mg or Nb that enhances or suppresses grain boundary kinetics, respectively. Application of this method to other ceramics seems possible, as the mechanisms for two-step sintering rely on the general features of kinetics and structural changes on the grain boundary,[1] which do not depend on the crystal structure/chemistry of Y_2O_3. One promising area to employ two-step sintering is in electroceramics,[2] where the trend of miniaturization is continuing, requiring ceramic capacitor and electromagnetic components in multi-layer-chip capacitors (MLCC) or multi-layer-chip inductors or beads (MLCI or MLCB) to become ever thinner and smaller.[3–5] As the grain size should be no more than one-tenth of the layer thickness in a multilayer assembly, as the layer thickness approaches micrometer and submicrometer range, nanograin ceramics will be in demand. Moreover, there is also a continuing trend to lower the sintering temperature of MLCC, MLCI, and MLCB in order to satisfy the co-firing requirement with Ag electrode (which melts at 961°C).[6,7] In this respect, the two-step sintering method offers an additional advantage as it requires a substantially lower sintering temperature than conventional sintering methods.

In this paper, we studied two prototypical electroceramics, perovskite-structured $BaTiO_3$ (BT) and spinel-structured $Ni_{0.2}Zn_{0.6}Cu_{0.2}Fe_2O_4$ (Ni–Zn–Cu) ferrite to assess the feasibility of two-step sintering for electroceramics. BT is extensively used as the base material for high dielectric constant capacitors, PTC resistors, transducers, and ferroelectric memories.[8] It is well known that above the Curie temperature (130°C), its structure is cubic and paraelectric, below which the structure is distorted and three ferroelectric polymorphs with nonzero dipole moments appear at various temperatures.[9,10] Thus far, the finest grain size of dense BT ceramics reported was 50 nm, fabricated by spark plasma sintering with a uniaxial hot-pressing pressure of 100 MPa.[11] In the case of ferrite, the present ceramic manufacturing technologies typically result in micrometer-sized grains and require sintering aids (typically Bi_2O_3 and V_2O_5), which form a liquid at the sintering temperature and induce compositional segregation in the fired ceramics.[4–7] The finest reported grain size of dense ferrite is about 1–2 μm fabricated by ultrafine powders,[12] but the need for fine grain ceramics has been recognized.

In the following we report how two-step sintering was successfully applied to obtain dense fine-grained BT and ferrite ceramics that sinter at low temperatures to $\geq 96\%$ of relative density without grain growth. To illustrate the utility of this approach, we limited our study to stoichiometric $BaTiO_3$ and Ni–Cu–Zn ferrite, without any sintering additive. In addition, as the Ti-rich BT composition is known to have a eutectic temperature of 1317°C, we kept the sintering temperatures well below this value to avoid any influence of liquid. Using two-step sintering, dense fine grain (35 nm for BT and 200 nm for ferrite) ceramics were obtained for the first time. In addition, the kinetics of two-step sintering was documented and compared with that of Y_2O_3, about which considerable understanding was already derived from our previous studies.[13] Lastly, we will demonstrate that the obtained structures of nanograin electroceramics possess salient features that ensure their ferroelectric and magnetic properties.

II. Experimental Procedures

High-purity BT nanocrystalline powders used here were synthesized by a modified oxalate precipitation method as described previously.[14] The starting materials were barium acetate ($Ba(CH_3COO)_2$), tetrabutyl titanate ($Ti(OC_4H_9)_4$), oxalic acid ($H_2C_2O_4$) as a precipitator, and alcohol as a solution medium. The precursor was calcined at different temperatures (650°–750°C) to produce phase pure nanocrystalline BT powders. The mean particle size, determined by transmission electron microscopy (TEM, TEM-200CX, JEOL, Tokyo, Japan) and X-ray diffraction (XRD, D/max, Rigaku Co., Tokyo, Japan), was 10–30 nm depending on the calcination temperature. The Ba/Ti atomic ratio was determined by X-ray fluorescence analysis to be 1 ± 0.003 for all the powders.

High-purity nanocrystalline ferrite powders with a composition of $Ni_{0.2}Cu_{0.2}Zn_{0.6}Fe_2O_4$ were prepared by a previously

M. Harmer—contributing editor

Manuscript No. 20593. Received May 23, 2005; approved July 29, 2005.
This work was supported by the Ministry of Sciences and Technology of China through 973-project under grant 2002CB613301 and 863-project under grant 2001AA325010, and by the US National Science Foundation, Grant Nos. DMR03-03458 and DMR00-79909.
†Author to whom correspondence should be addressed. e-mail: iweichen@seas.upenn.edu

Table I. Two-Step Sintering of $BaTiO_3$ (10 nm and 30 nm Powders) and NiCuZn Ferrite (10 nm Powders)

		After first-step sintering				After second-step sintering			
Sample	ρ_0 (%)	T_1 (°C)	t_1 (h)	ρ_1 (%)	G_1 (nm)	T_2 (°C)	t_2 (h)	ρ_2 (%)	G_2 (nm)
$BaTiO_3$-1†	61	950	0	86	33	900	2	98.0	35
$BaTiO_3$-2†	46	980	0	78	68	900	4	97.0	70
$BaTiO_3$-3	46	1100	0	73	148	900	20	96.2	150
$BaTiO_3$-4	46	1100	0	73	148	950	20	97.1	150
$BaTiO_3$-5	46	1150	0	78	200	900	20	96.3	200
$BaTiO_3$-6	46	1150	0	78	200	1000	20	97.2	200
$BaTiO_3$-7	46	1180	0	83	290	950	20	97.0	300
$BaTiO_3$-8	46	1180	0	83	290	1000	20	97.2	300
$BaTiO_3$-9	46	1200	0	87	495	850	20	96.0	500
$BaTiO_3$-10	46	1200	0	87	495	900	20	96.3	500
$BaTiO_3$-11	46	1200	0	87	495	1000	20	97.2	500
$BaTiO_3$-12	46	1200	0	87	495	1100	10	97.0	500
$BaTiO_3$-13	46	1230	0	90	795	850	20	97.5	800
$BaTiO_3$-14	46	1230	0	90	795	1000	20	98.0	800
Ferrite-1†	46	850	0	76	198	760	8	96.2	200
Ferrite-2†	46	850	0	76	198	800	6	97.1	200
Ferrite-3†	46	850	0	76	198	800	12	99.0	200
Ferrite-4†	46	890	0	81	397	750	6	97.2	400
Ferrite-5†	46	890	0	81	397	825	6	98.3	400
Ferrite-6†	46	890	0	81	397	825	8	100	400
Ferrite-7†	46	910	0	87	495	750	8	97.0	500
Ferrite-8†	46	910	0	87	495	800	6	98.1	500
Ferrite-9†	46	910	0	87	495	850	4	99.0	500
Ferrite-10†	46	930	0	91	792	800	4	99.2	800
Ferrite-11†	46	930	0	91	792	850	4	99.3	800
Ferrite-12†	46	930	0	91	792	870	4	99.2	800

†Ten nanometer powders.

reported citrate process.[12] The raw materials were reagent-grade iron nitrate, nickel acetate, copper acetate, citric acid, and ammonia. The citric precursor gel was dried, ignited, and combusted, or calcined at 600° – 800°C for 4 h, resulting in single-phase spinel-structured Ni–Cu–Zn ferrite nanocrystals with grain sizes from 10 to 60 nm according to TEM and XRD.

To prepare ceramics, powders were first milled and pressed into disks (10 mm in diameter and 1 mm thick). After isostatic pressing at 200 MPa to achieve a relative density of 46%, the green compacts were sintered using various two-step firing schedules. Typically, the sample was heated at 10°C/min to a higher temperature T_1 (950°–1250°C for BT, 850°–930°C for ferrite), then immediately cooled, at 30°C/min, to a lower temperature T_2 (1150°–850°C for BT, 750°–870°C for ferrite) for isothermal sintering with a dwelling time of 2–20 h (4–12 h for ferrite). Toroidal ferrite samples (20 mm outside diameter, 10 mm inside diameter, and 3 mm thickness) were also pressed and sintered in a similar way for magnetic measurements. To minimize particle coarsening during the first sintering step, one BT sample (#1 in Table I) was isostatically pressed at 2 GPa to achieve a higher green density of 61%, which allowed the use of a lower T_1.

The crystalline structures of the powders and ceramic samples were determined by XRD using a Rigaku diffractometer with Cu$K\alpha$ radiation. The microstructures of the ceramics were investigated using a Zeiss CSM-950 scanning electron microscopy (SEM, Carl Ziess Co., Oberkochen, Germany). The average grain size was determined by SEM micrographs of fractured or, for dense samples, polished surfaces using the linear intercept technique by counting at least 500 grains. TEM was also used to determine the particle size of powders. Final density (average of three duplicate pellets) was determined tobe within ± 0.01 g/cm^3 by the Archimedes method using distilled water as displacement liquid. The density after first-step sintering was estimated from the weight and dimension of duplicate specimens; the estimates were consistent with the data of dilatometry. In addition, Raman spectra of BT were recorded using a confocal microscopic Raman spectrometer (RM2000, Renishaw, U.K.) over the temperature range from −150° to 200°C. The saturation magnetization of ferrite ceramics was measured using an LDJ 9600 vibrating sample magnetometer, and their DC resistivity was determined using an HP 4040B meter (Palo Alto, CA).

III. Results and Discussion

(1) Characterization of Nanocrystalline Powders

An example of BT powders used in this study is shown in Fig. 1(A) for powders obtained after 750°C calcination. They have a homogeneous, nearly spherical shape with a size from 20 to 30 nm. This is consistent with XRD, which indicated an average crystallite size of 28.4 nm using estimation from the broadening of the (111) perovskite peak. (Here we assume a cubic perovskite structure as there was no splitting of (002) and (200) reflections).[11] They will be referred to as 30 nm BT powders below. Figure 1(B) shows an example of ferrite powders obtained after combustion, which had an average particle size of 8–10 nm. This is consistent with the XRD result, which indicated an average particle size of 10.3 nm. XRD also indicated a spinel structure with Ni/Cu/Zn occupying the A site and Fe occupying the B site. They will be referred to as 10 nm ferrite powders.

(2) Sintering and Microstructure

In successful two-step sintering, grain size should remain constant while density continues to increase, unlike in normal sintering in which final stage densification is always accompanied by rapid grain growth. This dramatic contrast of microstructure development was seen in both BT (Fig. 2(A)) and ferrite (Fig. 2(B)), where several grain size-density trajectories are depicted. It is clear that in both ceramics, grain growth during the second-step sintering ($T_2 < T_1$) was completely suppressed.

Table I lists some of the successful two-step sintering experiments using 10 or 30 nm BT powders and 10 nm ferrite powders. These experiments all achieved high density ($\geq$ 96%)

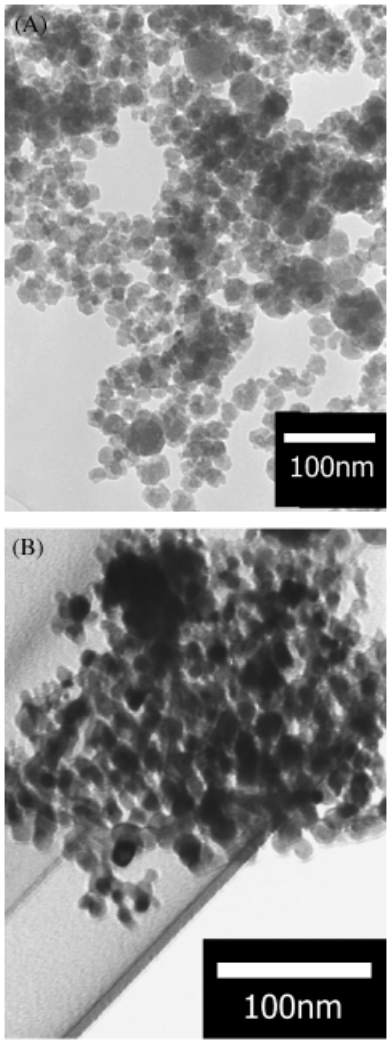

Fig. 1. Transmission electron microscopy image of (A) $BaTiO_3$ and (B) Ni–Cu–Zn ferrite nanocrystalline powders.

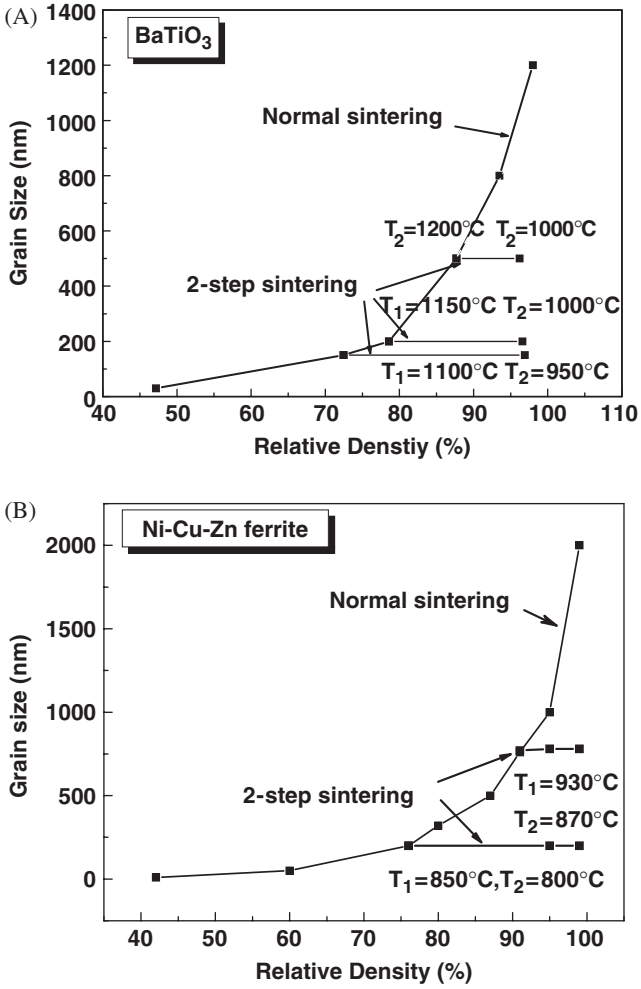

Fig. 2. Grain size versus density for (A) $BaTiO_3$ (30 nm powder) and (B) Ni–Cu–Zn ferrite (10 nm powder) specimens sintered by normal sintering and two-step sintering.

without grain growth in the second step. One sample (ferrite #6) even reached full density within the accuracy of our measurement. In contrast, in conventional sintering high density could not be reached at comparable temperatures. (For example, when 950°C was used to sinter BT for 20 h in conventional sintering, only 80% density was obtained.) These experiments also showed that, for BT, the lowest starting density for the second step was 73%. For ferrite, it was 76%. (Runs of lower starting density did not reach high density at T_2, and thus are not included in Table I. For example, for BT, when $T_1 = 1050$°C, $\rho_1 = 68\%$, $T_2 = 950/20$ h, final density = 85%, or when $T_1 = 1080$°C, $\rho_1 = 71\%$, $T_2 = 950$°C/20 h, final density = 89%.) For Y_2O_3, we found that a similar critical starting density of about 75% was required to allow sintering at T_2 to successfully proceed.[1,13] This is because below the critical density the pore size is so large, compared with the grain size, that pores are thermodynamically stable according to Kingery and Francois.[15]

For Y_2O_3, there is a kinetic window for second-step sintering, expressed in grain size and T_2, outside which high density ($\geq 96\%$) without grain growth can not be achieved even when the starting density is above critical.[2,13] Similar windows determined for BT and ferrite are shown in Fig. 3 in which the solid symbols indicate successful T_2 sintering, open symbols above the upper boundary indicate grain growth at T_2, and open symbols below the lower boundary indicate incomplete densification despite long soak times at T_2. As in the case of Y_2O_3, the slope of the upper boundary is positive, while the slope of the lower boundary is slightly negative. These similarities suggest very similar mechanisms operating in second-step sintering in all three systems, even though they have very different chemistry and crystal structures.[2,13] (In Y_2O_3, the same features of kinetic window were observed when different dopants—Mg and Nb—were introduced.) The upper boundary was explained by the increasing driving force for grain growth at smaller grain sizes, so the growth of finer grains begins at a lower temperature. The lower boundary was explained by the threshold effect on interface kinetics, which emerges at small grain sizes.[16–19] This effect diminishes at larger grain sizes, allowing the kinetic window to extend to lower temperatures.

Micrographs of BT and ferrite are shown in Figs. 4 and 5, respectively, for a number of dense ceramics obtained by two-step sintering and conventional sintering. In Fig. 4, the finest grain size (35 nm) is that of BT ceramic A, obtained using 10 nm powders (calcined at 650°C), cold-die-pressed at 2 GPa to 61% relative density, and then two-step sintered using $T_1 = 950$°C and $T_2 = 900$°C (2 h). Another fine grain BT ceramic, B (70 nm), was obtained using 10 nm powder, isostatic pressed at 200 MPa, and then two-step sintered using $T_1 = 980$°C and $T_2 = 900$°C (4 h). The coarsest grain size (1.2 μm) is that of ceramic F obtained using 30 nm powders, densified by normal sintering at 1200°C for 2 h (its grain size/density trajectory shown in Fig. 2(A)). In Fig. 5, the finest grain size (200 nm) is that of ferrite ceramic A. which was from 10 nm powders, two-step sintered at $T_1 = 850$°C and $T_2 = 800$°C (6 h). The coarsest grain size (2 μm) is that of ceramic E, which also used 10 nm powders, but densified by normal sintering at 900°C for 4 h (its grain-size/density trajectory shown in Fig. 2(B)). In addition to the larger

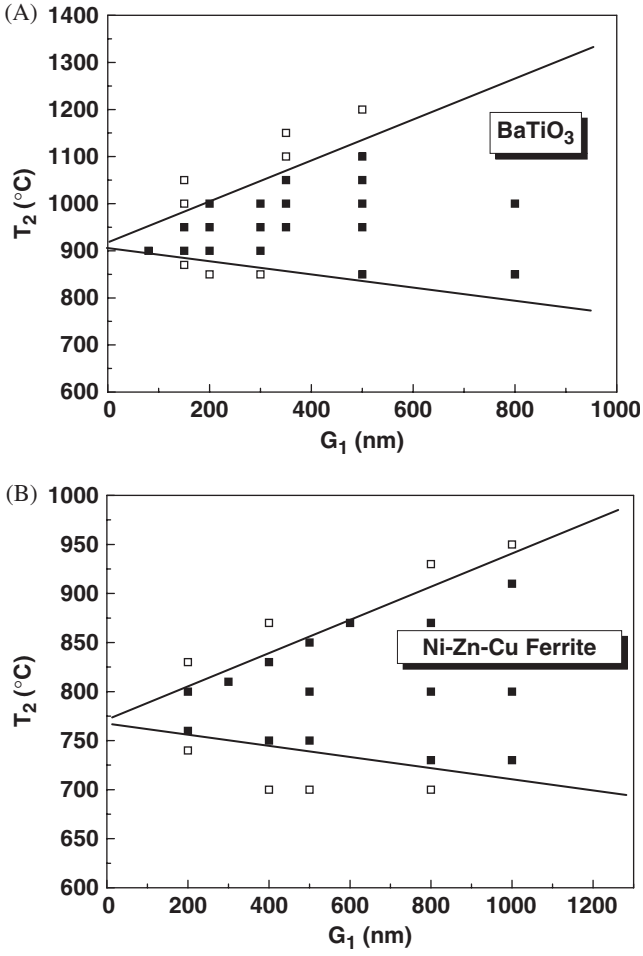

Fig. 3. Kinetic window (temperature T_2 and starting grain size used) for second-step sintering without grain growth for (A) $BaTiO_3$ and (B) Ni–Cu–Zn ferrite. Full symbols are ones reaching high density ($\geq$ 96%) without grain growth, open symbols unsuccessful ones with either grain growth (upper) or poor density (lower).

grain size, it exhibits an inhomogeneous microstructure with discontinuous grain growth resulting in some grains of more than 5 μm. As a further comparison, Fig. 5(F) shows the microstructure of a sample obtained by conventional processing, using normal sintering and powders from solid-state reactions. These microstructure comparisons clearly demonstrate the advantage of two-step sintering over other processing methods in obtaining fine-grained, uniform ceramics. Indeed, for both BT and ferrite, this was the first time that such fine grain sizes were reported for dense ceramics.

(3) Ferroelectric and Magnetic Structures of Nanocrystalline Ceramics

A full description of the physical properties of dense, nanograin ceramics sintered in this study will be reported elsewhere. Here we provide some evidence that their structures possess salient features that ensure their ferroelectric and magnetic properties.

To reveal the structure of dense nanograin BT ceramics, we used Raman spectra, which are shown in Fig. 6 for a 35 nm ceramic at different temperatures. According to Perry and Hall[20] and Laabidi *et al.*,[21] the 305 cm^{-1} (sharp) and 715 cm^{-1} bands are forbidden in cubic (C) symmetry, the peak position of the 240–270 cm^{-1} broad band discontinuously drops during the tetragonal to orthorhombic (T/O) transition, and the sharp multi-peak at 170–190 cm^{-1} band is a rhombohedral (R) characteristic, although in both O and T symmetries it still manifests as a weak, diffuse feature. Meanwhile, the small positive peak at 487 cm^{-1} is also a characteristic R band. From Fig. 6, we can then definitely identify that in the 35 nm ceramic R symmetry exists at −150°C and there is a T/O transition at 50°C, which is sufficient to establish the existence of all three ($T/O/R$) symmetries. In addition, the nominally C spectrum at 200°C still has weak features at 305 and 715 cm^{-1} indicating T remnants. Therefore, the C/T transition was rather diffuse in this nanograin ceramic. The above Raman features provide evidence that there is a driving force for structure distortion of the same type that occurs in coarse grain BT. Therefore, nanograin ceramics should be capable of ferroelectricity at least on the local level. This has been verified in our ongoing study by piezoelectric imaging, dielectric constant, and high-resolution XRD.[22]

Evidence that nanograin ferrite ceramics are magnetically active was provided by measurements of saturation magnetization

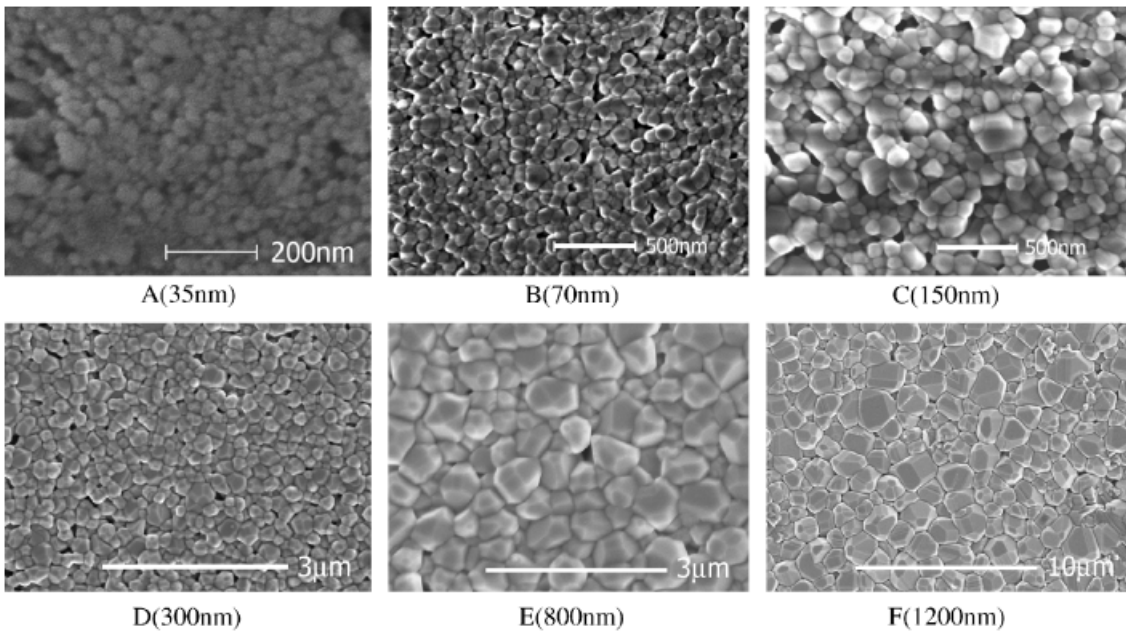

Fig. 4. Scanning electron microscopy micrographs of dense $BaTiO_3$ ceramics prepared by two-step sintering. (A) 35 nm (T_1 = 950°C, T_2 = 900°C/2 h), (B) 70 nm (T_1 = 980°C, T_2 = 900°C/4 h), (C) 150 nm (T_1 = 1100°C, T_2 = 900°C/20 h), (D) 300 nm (T_1 = 1180°C, T_2 = 950°C/20 h), (E) 800 nm (T_1 = 1230°C, T_2 = 1000°C/20 h), and normal sintering (F) 1200 nm (T = 1200°C/2 h).

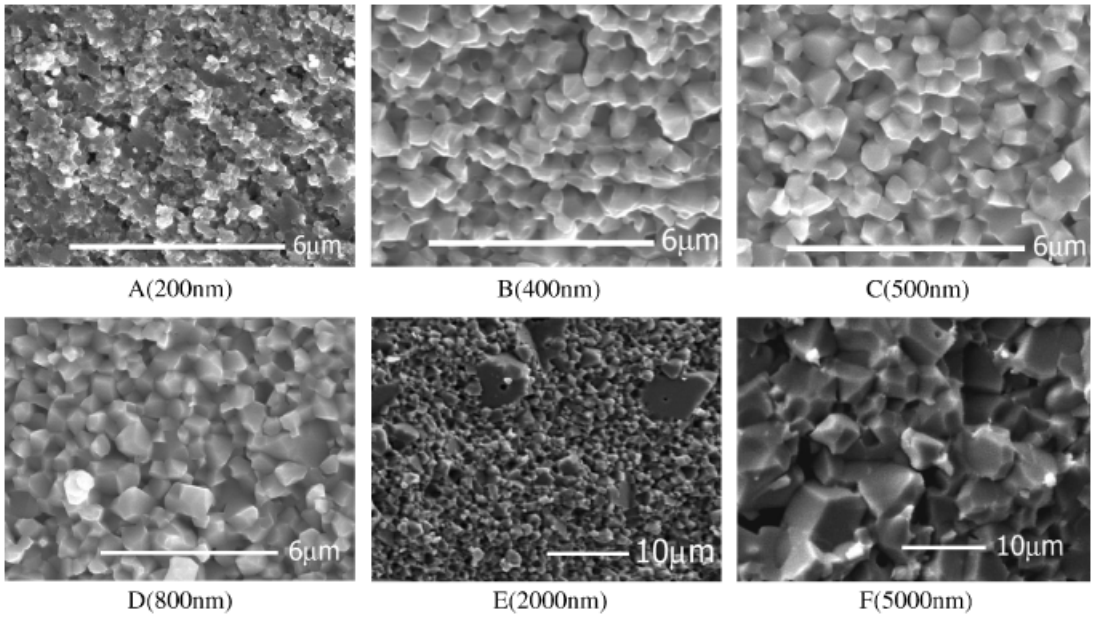

Fig. 5. Scanning electron microscopy micrographs of dense NiCuZn ferrite made from 10 nm powders, by two-step sintering, (A) 200 nm ($T_1 = 850°C$, $T_2 = 800°C/6$ h), (B) 400 nm ($T_1 = 890°C$, $T_2 = 825°C/8$ h); this sample reached full density (ferrite #6 in Table I), (C) 500 nm ($T_1 = 910°C$, $T_2 = 850°C/4$ h), (D) 800 nm ($T_1 = 930°C$, $T_2 = 850°C/4$ h), and normal sintering (E) 2000 nm (900°C/4 h). Also shown is ferrite made from powders of solid-state reactions, (F) 5000 nm (900°C/4 h).

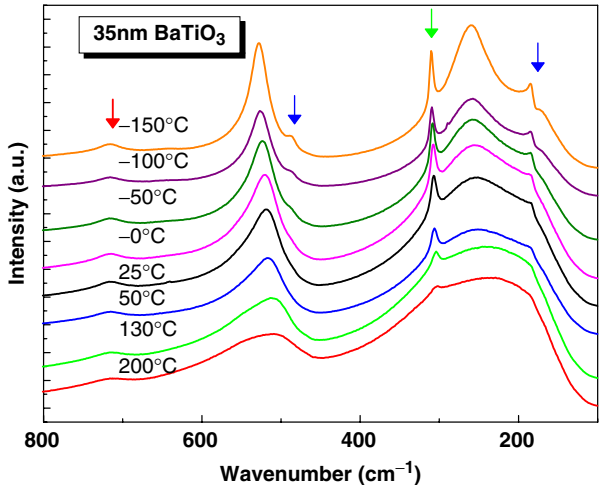

Fig. 6. Raman spectra of 35 nm $BaTiO_3$ ceramics. Distinguishing features (see text) marked by arrows.

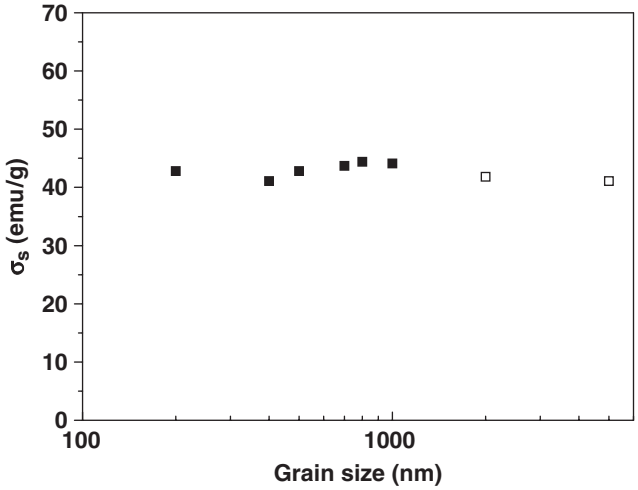

Fig. 7. Saturation magnetization (σ_s) versus grain size for ferrite ceramics. Solid symbols for two-step sintering, open ones for normal sintering.

(σ_s). As shown in Fig. 7, σ_s is independent of grain size and processing method, indicating similar magnetic interactions at the atomic level. This would be assured if the same spinel structure with the same pattern of site occupancy by different cations is adopted. Because of the smaller grain size and more uniform composition/microstructure, the resistance of nanograin ferrites all exceeded 10^{10} $\Omega \cdot$cm, which is an additional advantage for ferrite applications.

IV. Conclusions

1. Two-step sintering was used to sinter $BaTiO_3$ and Ni–Cu–Zn ferrite ceramics to high density with unprecedentedly fine grain size, by suppressing grain growth in the final stage of densification. Second-step densification temperatures as low as 900°C for $BaTiO_3$ and 760°C for Ni–Zn–Cu apparently sufficed.
2. The processing windows for successful second-step sintering to achieve high density without grain growth were identified for $BaTiO_3$ and Ni–Cu–Zn ferrite ceramics. They share the same features as the one previously determined for undoped and doped Y_2O_3.
3. Dense $BaTiO_3$ ceramics with a grain size of 35 nm undergo distortions from cubic to various low-temperature ferroelectric structures. Dense fine grain Ni–Cu–Zn ferrite ceramics have the same saturation magnetization as their coarse grain counterparts.

References

[1]I.-W. Chen and X.-H. Wang, "Sintering Dense Nano-Crystalline Ceramics Without Final Stage Grain Growth," *Nature*, **404**, 168–71 (2000).
[2]N. Setter and R. Waser, "Electroceramic Materials," *Acta Mater.*, **48**, 151–78 (2000).
[3]H. Kishi, Y. Mizuno, and H. Chazono, "Base-Metal Electrode-Multilayer Ceramic Capacitors: Past, Present and Future Perspectives," *Jpn. J. Appl. Phys.*, **42**, 1–15 (2003).
[4]X. He, M. Xiong, Z. Ling, and Q. Qiu, "Low-Temperature Sintering of Ni-CuZn Ferrite for Multilayer-Chip Inductor," *J. Inorg. Mater.*, **14** [1] 71–7 (1999).
[5]T. Yamaguchi and M. Shinagawa, "Effect of Glass Addition and Quenching on the Relation Between Inductance and External Compressive Stress in Ni–Cu–Zn Ferrite Glass Composites," *J. Mater. Sci.*, **30** [2] 504–8 (1995).
[6]J. Y. Hsu, W. S. Ko, and C. J. Chen, "The Effect of V_2O_5 on the Sintering of NiCuZn Ferrite," *IEEE Trans. Magn.*, **31** [6] 3994–6 (1995).
[7]W.-G. Qu, X.-H. Wang, and L.-T. Li, "Preparation and Performance of NiCuZn–Co_2Z Composite Ferrite Material," *J. Magn. Magn. Mater.*, **257** [2–3] 284–9 (2003).

[8]G. H. Hertling, "Ferroelectric Ceramics: History and Technology," *J. Am. Ceram. Soc*., **82** [4] 797–818 (1999).
[9]M. H. Frey, Z. Xu, P. Han, and D. A. Payne, "The Role of Interfaces on an Apparent Grain Size Effect on the Dielectric Properties for Ferroelectric Barium Titanate Ceramics," *Ferroelectrics*, **206** [1–4] 337–53 (1998).
[10]G. Alrt, D. Hennings, and G. De With, "Dielectric Properties of Fine-Grained Barium Titanate Ceramics," *J. Appl. Phys*., **58** [4] 1619–25 (1985).
[11]Z. Zhao, V. Buscaglia, M. Viviani, M. T. Buscaglia, L. Mitoseriu, A. Testino, M. Nygren, M. Johnsson, and P. Nanni, "Grain Size effects on the Ferroelectric Behavior of Dense Nanocrystalline $BaTiO_3$ Ceramics," *Phys. Rev. B*, **70**, 024107 (2004).
[12]X.-H. Wang, W.-G. Qu, and L.-T. Li, "Investigation of NiCuZn Ferrite with High Performance Derived from Nano Ferrite Powders," *Ceram. Trans*., **129**, 211–7 (2002).
[13]X.-H. Wang, P.-L. Chen, and I.-W. Chen, "Two-Step Sintering of Ceramics with Constant Grain size, I. Y_2O_3," *J. Am. Ceram. Soc*., **89** [2] 431–7 (2006).
[14]X.-H. Wang, R.-Z. Chen, L.-T. Li, and Z.-L. Gui, "Synthesis and Properties of Barium Titanate Based X7R Ceramics by Chemical Method," *Ferroelectrics*, **262** [1–4] 1225–30 (2001).
[15]W. D. Kingery and B. Francois, "The Sintering of Crystalline Oxides: Interactions between Grain Boundaries and Pores," p. 471 in *Sintering and Related Phenomena*, Edited by G. C. Kuczynski, N. S. Hooton, and C. F. Gibbon. Gordon and Breach, New York, 1967.
[16]J. W. Cahn, "Theory of Crystal Growth and Interface Motion in Crystalline Materials," *Acta Metall*., **8** [8] 554–62 (1960).
[17]B. Burton, "Interface-Reaction-Controlled Diffusional Creep. A Consideration of Grain-Boundary Dislocation Climb Sources," *Mater. Sci. Eng*., **10** [1] 9–14 (1972).
[18]R. M. Cannon, W. H. Rhodes, and A. H. Heuer, "Plastic Deformation of Fine-Grained Alumina: I. Interface-Controlled Diffusional Creep," *J. Am. Ceram. Soc*., **63** [1–2] 48–53 (1980).
[19]E. Arzt, M. F. Ashby, and R. A. Verrall, "Interface-Controlled Diffusional Creep," *Acta Metall*., **31** [12] 1977–89 1983.
[20]C. H. Perry and D. B. Hall, "Temperature Dependence of the Raman Spectra of $BaTiO_3$," *Phys. Rev. Lett*., **15**, 700–2 (1965).
[21]K. Laabidi, M. D. Fontana, and B. Jannot, "Underdamped Soft Phonon in Orthorhombic $BaTiO_3$," *Solid. State Commun*., **76**, 765–8 (1990).
[22]X.-H. Wang, X.-Y. Deng, W. Dmowski, Y.-D. Wang, L.-T. Li, and I.-W. Chen, "Low-Temperature Transitions in Nanograin Barium Titanate," *Appl. Phys. Lett*., (2004) to be published. □